



EUROfusion

WPEDU-PR(18) 21195

A Rakha et al.

Modelling of Beam driven Alfvén modes in TJ-II plasmas

Preprint of Paper to be submitted for publication in
Nuclear Fusion



This work has been carried out within the framework of the EUROfusion Consortium and has received funding from the Euratom research and training programme 2014-2018 under grant agreement No 633053. The views and opinions expressed herein do not necessarily reflect those of the European Commission.

This document is intended for publication in the open literature. It is made available on the clear understanding that it may not be further circulated and extracts or references may not be published prior to publication of the original when applicable, or without the consent of the Publications Officer, EUROfusion Programme Management Unit, Culham Science Centre, Abingdon, Oxon, OX14 3DB, UK or e-mail Publications.Officer@euro-fusion.org

Enquiries about Copyright and reproduction should be addressed to the Publications Officer, EUROfusion Programme Management Unit, Culham Science Centre, Abingdon, Oxon, OX14 3DB, UK or e-mail Publications.Officer@euro-fusion.org

The contents of this preprint and all other EUROfusion Preprints, Reports and Conference Papers are available to view online free at <http://www.euro-fusionscipub.org>. This site has full search facilities and e-mail alert options. In the JET specific papers the diagrams contained within the PDFs on this site are hyperlinked

Modelling of Beam-driven Alfvén modes in TJ-II plasmas

Allah Rakha^{1*}, M.J. Mantsinen^{1,2}, A.V. Melnikov^{3,4}, S. E. Sharapov⁵, D. A. Spong⁶, A. Cappa⁷, A. López-Fraguas⁷, F. Castejón⁷, A. Gutiérrez-Millá¹, J. L. de Pablos⁷, X. Sáez¹

¹ Barcelona Supercomputing Center, 08034, Barcelona, Spain

² ICREA, Pg. Lluís Companys 23, 08010 Barcelona, Spain

³ National Research Center 'Kurchatov Institute', 123182, Moscow, Russia

⁴ National Research Nuclear University MEPhI, 115409, Moscow, Russia

⁵ CCFE, Culham Science Centre, Abingdon, OX14 3DB, UK

⁶ Oak Ridge National Laboratory, TN, 37831, USA

⁷ Fusion National Laboratory, CIEMAT, 28040, Madrid, Spain

E-mail: allah.rakha@bsc.es

August 2018

Abstract. The properties of hydrogen Neutral Beam Injection (NBI) driven Alfvén eigenmodes (AEs) in the TJ-II flexible heliac are investigated using a reduced MHD model coupled to a realistic MHD equilibrium. The simulation results of AEs frequency and radial localization are found to be broadly consistent with experimental observations. The simulation results show that an AE with the same poloidal and toroidal harmonics persists under small variations in on-axis iota values, which is consistent with the experimental observations. The corresponding wave-particle resonance maps suggest the possibility of describing the nonlinear evolution of the AEs in TJ-II by a sum of two ion populations with different weighting factors, one of which is dominated by drag and the other by diffusion.

Keywords: Alfvén eigenmodes (AEs), steady and chirping modes, drag and diffusion of fast ions

Submitted to: *Nucl. Fusion*

1. Introduction

Fast particle driven Alfvénic instabilities can have a crucial impact on the efficient heating of burning fusion plasmas. Stellarators are disruption-free steady-state helical devices aiming at sustained magnetic fusion power. To solve the problem of plasma self-heating with fusion-born alpha particles, the transport properties of the alpha particles must be known with a high level of confidence. Alfvén eigenmodes (AEs) driven unstable by fast particles represent a significant uncertainty in predicting the transport of alpha particles. They must be investigated in detail in present-day experiments since they may lead to losses of fast ions on plasma-facing components (PFCs) and decrease the ignition margin. Modelling studies of AEs in three-dimensional (3D) magnetic fusion systems are of primary importance due to observed 3D effects such as coupling effects across different toroidal mode numbers in both tokamaks [1] and stellarators [2]. The calculation of Alfvén continuum and eigenmode structures are the first steps to take in order to compare theory and experiment for the Alfvén stability and confinement of energetic particles (EPs), enabling comparisons of modelling and experimental results to assess the validity of the AE physics models. Among the 3D magnetic fusion devices, the physics of AEs in stellarators is quite different from toroidally axisymmetric devices such as tokamaks due to different mode couplings and mode families corresponding to the number of field period (N_{fp}) in the toroidal direction of stellarators.

A number of numerical tools of varying complexity and approaches have been developed to investigate Alfvénic instabilities and wave-particle interaction in 3D geometries. For 3D linear ideal MHD continuum studies, the COBRAS code [3] based on the analytic derivation of the metric tensor coefficients and CONTI code [4] by incorporating the coupling between Alfvén and sound waves in stellarator plasmas have been developed. For the investigations of properties of AEs and interaction with EPs in 3D magnetic fusion systems the CKA code [5] based on reduced MHD and finite Larmor radius effects and the BOA code [3] also based on a reduced-MHD model solving an eigenvalue problem with symmetric matrices have been developed. In this paper, for 3D flexible heliac TJ-II plasmas, the shear Alfvén continuum calculations are performed with the STELLGAP code [6] based on the theoretical explanations given in [7]. In the next step, the analysis of AEs is carried out with the AE3D [8], a clustered frequency model for the computation of eigenmodes centered on a specified target frequency. The centered frequency algorithm of the AE3D code is based on application of the JacobiDavidson method to a reduced MHD model [9]. This tool is more efficient by a factor of 10^2 - 10^3 in finding a subset of eigenmodes around a unique input frequency as compared with conventional methods. The 3D numerical tools employed for the investigation of AE instabilities have been successfully applied previously to investigate such instabilities in MST [10], LHD [11] and TJ-II [12–14].

In the present work, the experimental findings in [15] have motivated the investigation of AE properties in a dynamic configuration scan (iota varies during discharge) of TJ-II stellarator. The iota, also known as rotational transform, in

stellarators is equivalent to the inverse of the safety factor q , where q is equal to the number of poloidal transits per single toroidal transit of a field line on a toroidal flux surface. During the iota scan obtained by changing an external coil current, nonlinear evolution of the beam-driven AEs changed from bursting amplitude-sweeping frequency to steady amplitude-steady frequency, and then back. The understanding of this behaviour is of importance because it would have direct implications on the type of alpha-particle losses (pulsating or steady-state) in future 3D magnetic fusion systems.

This paper is organized as follows: Experimental observations for the modelling of modes are given in section 2. Section 3 describes the 3D numerical model used. Section 4 explains the equilibrium calculation in TJ-II plasmas for TJ-II dynamic discharges. Furthermore, the section 5 presents the simulation results for both iota ramp-down and ramp-up cases. In section 6 the results for wave-particle resonances in TJ-II are presented. Section 6 also includes a discussion on two fast particle populations with different weighting factors as a possible explanation for the observed non-linear evolution of the modes. Finally, section 7 includes a summary and concluding remarks.

2. Experimental Observations

TJ-II is a four field period (N_{fp}) = 4 flexible heliac with a low magnetic shear, equilibrium magnetic field $B_0 = 0.95$ T, major radius $R_0 = 1.5$ m and averaged minor radius $\bar{a} \leq 0.22$ m. The flexibility of TJ-II allows investigation of the properties of AEs by setting-up static discharges, i.e. discharges with a constant equilibrium [16], as well as dynamic discharges, i.e. discharges with a time-varying equilibrium scan that shows a changing rotational transform [17]. In the TJ-II experiments considered here, fast hydrogen ions are introduced in hydrogen plasmas using two Neutral Beam Injection (NBI) systems, each with a beam energy $E_{NBI} = 32$ keV and injected power $P_{NBI} \leq 0.5$ MW. These beam particles have a velocity of $V_{NBI} \sim 2.5 \times 10^6$ m/s satisfying $V_{NBI} \geq V_A/3$ where V_A is the Alfvén velocity.

In our investigations of AE properties in TJ-II, we focus on two low density ($\bar{n}_e = 1.0 \times 10^{19} \text{ m}^{-3}$) L-mode discharges 29834 and 29839, for which $V_A = 5.12 \times 10^6$ m/s. In both discharges, coexisting chirping and steady Alfvénic modes are observed. The observed Alfvénic activity is shown in the corresponding spectrograms in figure 1 together with the zoom of observed modes revealing both chirping and steady modes. In discharges #29834 and #29839, the magnetic configuration was scanned dynamically, including iota profile, by varying the currents in the external coils during the discharges, keeping all the other experimental settings unchanged. In discharge #29839, the iota was ramped up, while in discharge #29834 the iota was ramped down. A heavy ion beam probe (HIBP) [13] was used to investigate AEs. The HIBP data show that modes are located around $\rho = 0.55$ and the frequencies of modes are around 295 kHz, where ρ is a normalized radial parameter defined as $\rho = \sqrt{\psi_{tor}}$ and ψ_{tor} is the normalized toroidal flux. The frequencies of these modes are confirmed with magnetic diagnostics and by using cross coherence between different signals.

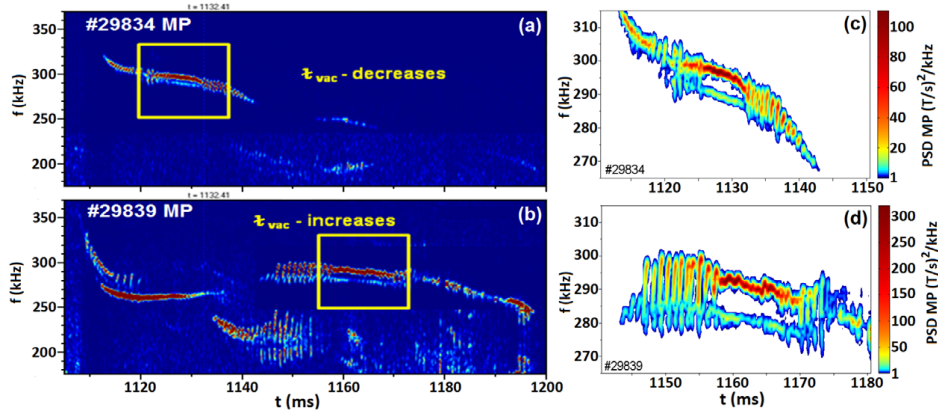


Figure 1. Time evolution of AE modes with iota variation. (a) Poloidal field (B_{pol}) spectrograms, measured by a Mirnov Probe (MP) in shot #29834 with iota ramp-down. (b) Poloidal field (B_{pol}) spectrograms, measured by MP in shot #29839 with iota ramp-up. Figures (c) and (d) show zooms of (a) and (b), respectively, focusing in the time period of the mode transformation [15].

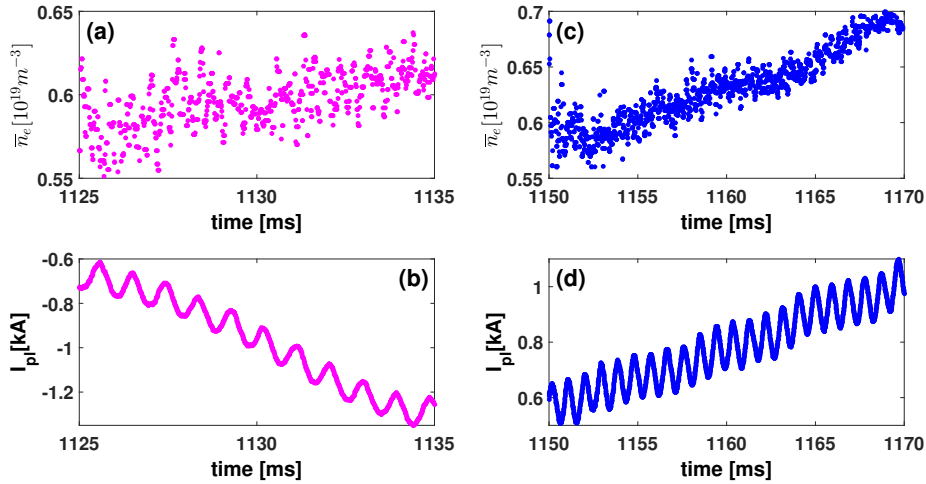


Figure 2. The temporal evolution of plasma density averaged over the central chord line and plasma current. (a) Line averaged plasma density and (b) plasma current for the discharge #29834 and (c) line averaged plasma density and (d) plasma current for the discharge #29839.

The temporal evolution of the central plasma density and current shows small variations during the time windows of mode transformation as shown in figure 2. While these variations are small, they can contribute to the details of the mode behaviour. Their effects have been studied in detail in other TJ-II experiments [17]. In the numerical modelling presented in this paper, we have only retained the dominant iota variation in time as described later in section 4 while assuming that the variation in the plasma density and current in time has a negligible effect on the mode behaviour. As an extension of this work, we are investigating the effect of plasma current on the iota

profile and thereby on AEs. Preliminary results with monotonic and non-monotonic iota profiles caused by finite plasma current are presented [20].

3. Mathematical model

In this section, we briefly describe the mathematical model for the 3D modelling of AEs. First, the Alfvén continuum solver STELLGAP [6] is presented, followed by the discussion of the clustered frequency model AE3D [8].

3.1. The continuum solver STELLGAP

The continuum solver STELLGAP is based on the Alfvén continuum equation derived in [7] for the stellarator geometry. In the incompressible limit for low β plasmas it is given as,

$$\mu_0 \rho \omega^2 \frac{|\nabla\psi|^2}{B^2} \xi_s + \vec{B} \cdot \vec{\nabla} \left\{ \frac{|\nabla\psi|^2}{B^2} (\vec{B} \cdot \vec{\nabla}) \xi_s \right\} = 0 \quad (1)$$

where the magnetic surface displacement is $\xi_s = \xi(\vec{B} \times \vec{\nabla}\psi)/|\nabla\psi|^2$. This equation can be represented for different poloidal (m) and toroidal (n) mode numbers (m, n) as a symmetric matrix eigenvalue equation,

$$\omega^2 \overleftrightarrow{A} \vec{x} = \overleftrightarrow{B} \vec{x} \quad (2)$$

where \vec{x} is a vector having different components of ξ_s . With this set of equations, the Alfvén continuum is computed by STELLGAP for all relevant modes numbers (m, n) using the DGEGV routine from the IBM ESSL library.

3.2. AE3D Eigenmode solver

The eigenmode solver AE3D [8] calculates Alfvén eigenmodes in 3D equilibria using a reduced MHD model of shear Alfvén waves for three-dimensional toroidal plasmas. In this reduced system, the two basic laws, i.e. the ideal MHD Ohms law and the 3D vorticity equations, lead to an eigenvalue problem.

$$\omega^2 \nabla \cdot \left(\frac{1}{V_A^2} \nabla \phi \right) + (\vec{B} \cdot \vec{\nabla}) \left\{ \frac{1}{B} \nabla^2 \left(\frac{\vec{B}}{B} \cdot \nabla \phi \right) \right\} + \nabla \zeta \times \nabla \left(\frac{\vec{B}}{B} \cdot \nabla \phi \right) \cdot \nabla \frac{J_{\parallel 0}}{B} = 0 \quad (3)$$

This eigenvalue problem is solved in AE3D using a Jacobi-Davidson style QZ (JDQZ) algorithm [18]. AE3D achieves faster performance by pre-specifying an eigenvalue (frequency) centre for the eigenmode search and by computing with JDQZ a subset of all eigenvalues.

4. Equilibrium for TJ-II dynamic plasmas

We start our investigations with equilibrium reconstructions for TJ-II discharges #29834 and #29839. We perform the equilibrium reconstruction calculations using the VMEC

code [19] by taking into account the appropriate TJ-II magnetic geometries. VMEC constructs an equilibrium by employing a variational method to find a minimum of the system energy.

Since the experimental findings show a time evolution between chirping and steady types of AEs and back in both cases, we focus our analysis on a number of time slices which exhibit different mode activity in both discharges. The main part of our simulations is carried out for time slices $t = 1130$ and 1135 ms in discharge #29834, corresponding to steady and chirping modes, respectively, and for time slices $t = 1150$ and 1160 ms in discharge #29839, corresponding to chirping and steady modes, respectively. In the rest of the paper, our discussion relates to the results for these time slices unless otherwise noted. However, we have also considered additional time slices to check whether the trends emerging from the modelling hold in general. In the following sections, we will clearly indicate when we are discussing the results of these additional time slices instead the time slices given above.

The TJ-II fixed-boundary equilibria have been reconstructed under experimental constraints for both discharges at the chosen times. The vacuum rotational transform ($\iota/2\pi$) profiles for the VMEC reconstructed equilibria based on experimentally selected magnetic configuration for both discharges at the selected times are shown in figure 3. The resulting iota profiles increase monotonically in radius and range between $1.63 \geq \iota/2\pi \leq 1.76$.

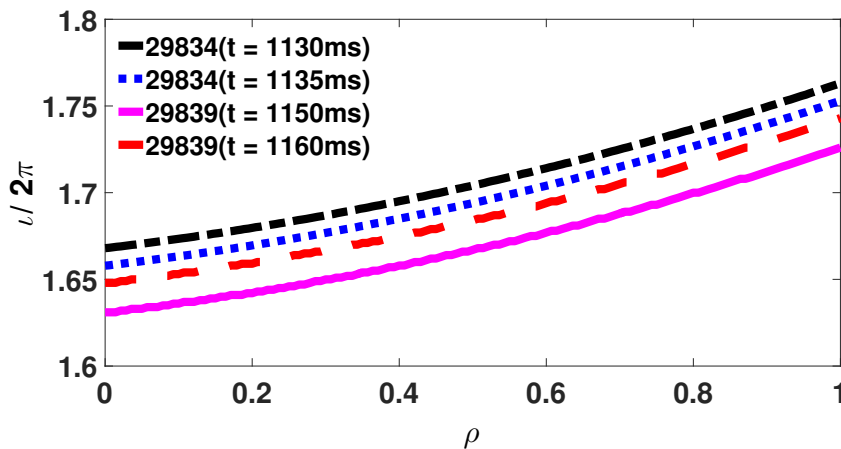


Figure 3. *Iota profiles for the four selected time slices for both iota ramp-up and ramp-down discharges. These iota profiles are calculated with the VMEC converged equilibrium.*

5. Simulation results and discussions

After setting-up the plasma equilibrium using VMEC, the STELLGAP simulations were performed to compute the Alfvén continuum. For the dominant toroidal mode number (n), the results of shear Alfvén spectra are plotted for both discharges at the

selected times. To illustrate the computed Alfvén eigenmode properties, the simulated electrostatic potential versus normalized radius from AE3D code are presented case by case.

5.1. Simulation results for the ramp-down of iota in TJ-II

Alfvén continua calculated by the STELLGAP code for the discharge #29834 at $t = 1130$ and 1135 ms are presented in figure 4, where the dominant toroidal mode number (n) is highlighted by colour coding. In both shear Alfvén spectra, there are clear gaps visible about 250-350 kHz, which are considered as an initial frequency target for the search of AEs. The AEs are computed with the AE3D code, and it is found that two prominent modes with $m = 11$ and $n = 19$ and $m = 9$ and $n = 15$ appear with different frequencies of 276 kHz shown in figure (5a) and 256 kHz figure (5b) at similar radial location $\rho = 0.65$ in the steady AE-frequency case. Likewise, in the chirping AE-frequency case, AEs with same mode numbers and higher frequencies of 292 and 287 kHz are found at radial location $\rho = 0.75$ as shown in figure 6. Comparison of results in the iota ramp-down case shows that there is a small increase in frequencies from the steady to chirping mode transition and the modes are also displaced radially outwards. The observed frequency increase is explained by the decrease of the density at the outer radial positions.

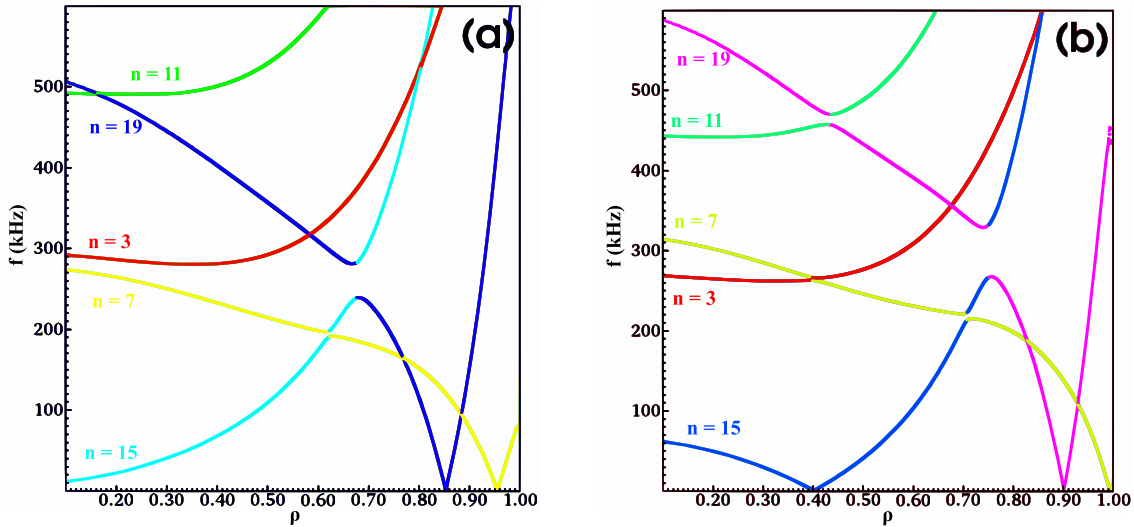


Figure 4. Shear Alfvén spectra for discharge #29834. (a) Alfvén continuum structures for steady mode and (b) Alfvén continuum structures for the chirping mode.

The radial extent $\delta\rho$ of AEs was calculated as the Full Width at Half Maximum (FWHM) of the simulated potential structures. For both discharges, our results show that the radial extent of AEs shrinks from $\delta\rho = 0.11$ in the chirping phase to a minimum of $\delta\rho = 0.04$ during the steady phase. Thus, it can be suggested that the modes calculated during steady phase are relatively more peaked than those in the chirping phase, however for some modes, $\delta\rho$ has no significant difference between the steady phase and the chirping phase. Simulations for an additional earlier time slice $t = 1125$

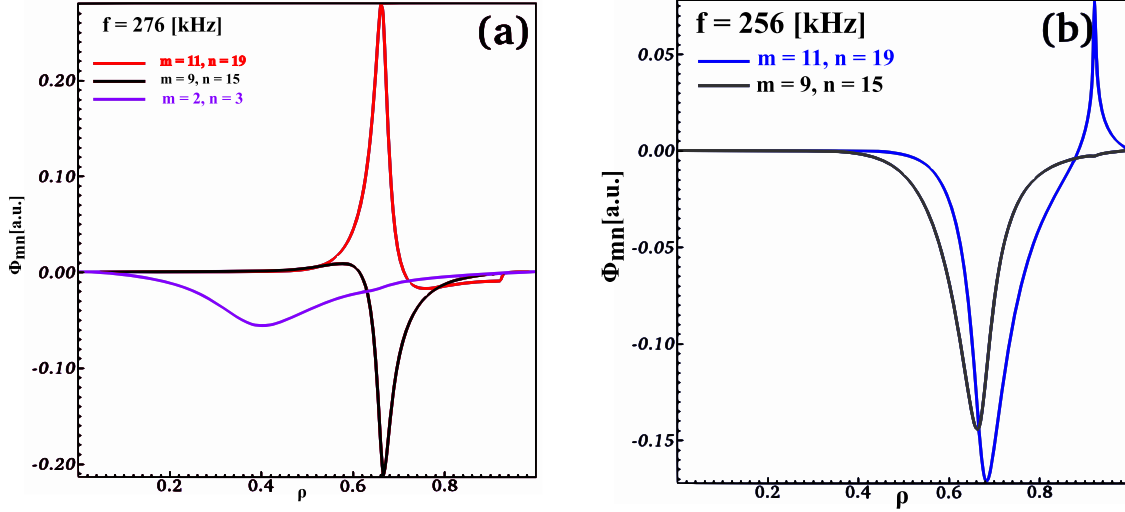


Figure 5. Alfvén eigenmodes for the steady mode in discharge #29834. (a) An AE with three different sets of prominent mode numbers (m, n) having single dominant frequency 276 kHz and (b) AE with two different sets of prominent mode numbers (m, n) having single dominant frequency of 256 kHz.

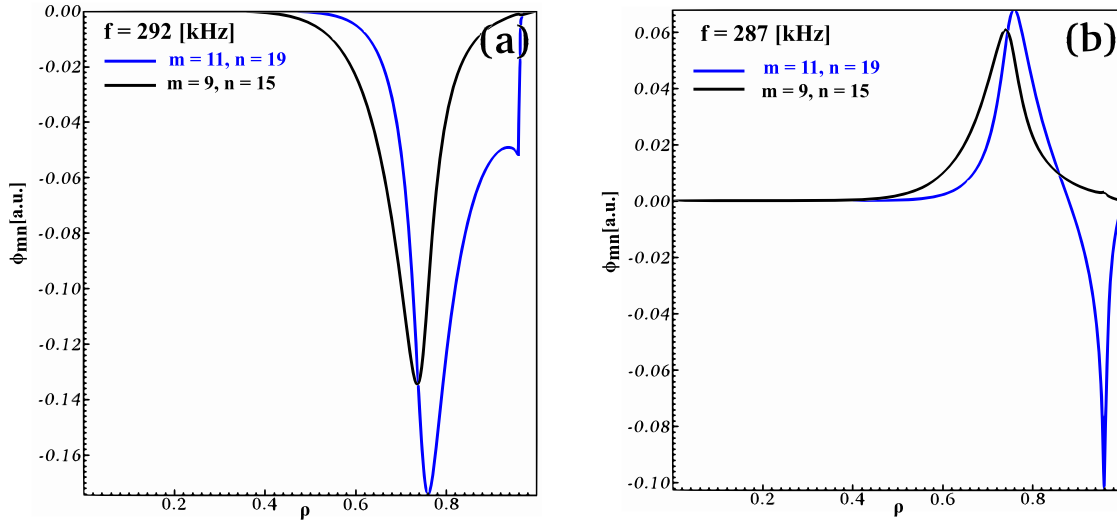


Figure 6. Alfvén eigenmodes for the chirping mode in discharge #29834. (a) An AE with two different sets of prominent mode numbers (m, n) having single dominant frequency 292 kHz and (b) AE with two different sets of prominent mode numbers (m, n) having single dominant frequency of 287 kHz.

ms show the same prominent modes as for the time slices $t = 1130$ and 1135 ms. At $t = 1125$ ms, the mode frequencies are 246 and 232 kHz and the mode is radially located at $\rho = 0.6$. In conclusion, according to our modelling results, when the iota is ramped down in discharge #29834 the prominent AE remains the same while its frequency increases slightly and it moves to larger ρ . The modelled evolution of the mode frequency is in agreement with experimental observations.

5.2. Simulation results for the ramp up of iota in TJ-II

In section 5.1, we have shown the results of our modelling for the TJ-II discharge #29834 with the ramp down of the iota. In this section we consider TJ-II discharge #29839 with the opposite time variation in iota, i.e. iota ramp-up. Similar to discharge #29834, here we also compute the Alfvén continuum for discharge #29839 using STELLGAP at $t = 1150$ and 1160 ms exhibiting a chirping and steady mode, respectively. Figure 7 displays the calculated continua with different colours representing the different dominant toroidal mode numbers. The clear open gaps in the continuum structures at the cross coupling of $n = 17$ and 13 can be seen in both cases ranging in the frequencies of 300 to 220 kHz with radial localization of $\rho = 0.7$ to $\rho = 0.6$. Again, the frequency change is explained by the lower densities at outer positions.

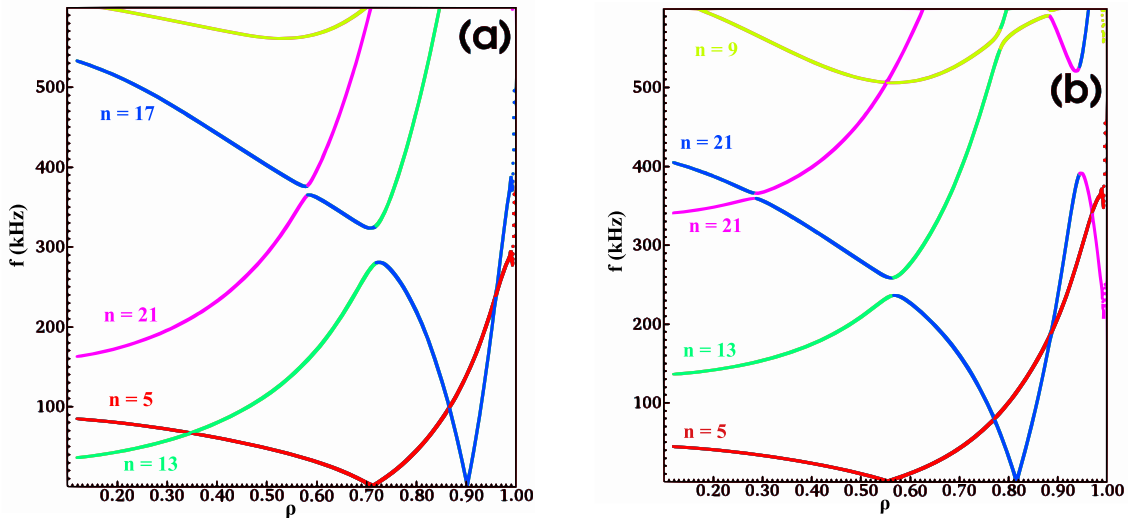


Figure 7. Shear Alfvén spectra for discharge #29839. (a) Alfvén continuum structures for the chirping mode and (b) Alfvén continuum structures for the steady mode.

Again AEs are computed using the AE3D code and plotted in figures 8 and 9 for the chirping and steady modes respectively. It is interesting to note that in both cases the two observed modes remain same, i.e. their mode numbers $m = 10$ and $n = 17$ and $m = 8$ and $n = 13$ are the unchanged for the chirping and steady mode phases. However, there is a decrease in the modes frequencies from 289 and 316 kHz in the chirping case shown in figure 8 to 254 kHz in the case of steady mode shown in figure 9, explained by the higher density values at the mode position. Moreover, there is a radial inward movement of the mode from $\rho = 0.7$ to $\rho = 0.55$ when the AE structure changes from a chirping mode to steady mode. We consider the modes with $m = 10$ and $n = 17$ and $m = 8$ and $n = 13$ as the prominent modes consistent with experimental results, despite the slight decrease in their frequency from 289 to 254 kHz.

Similarly as for the case with the iota ramp-down, we have extended our simulations for discharge #29839 to an additional time slice $t = 1170$ ms with chirping AE activity and at higher iota value. At this time slice, our results show that there are also two

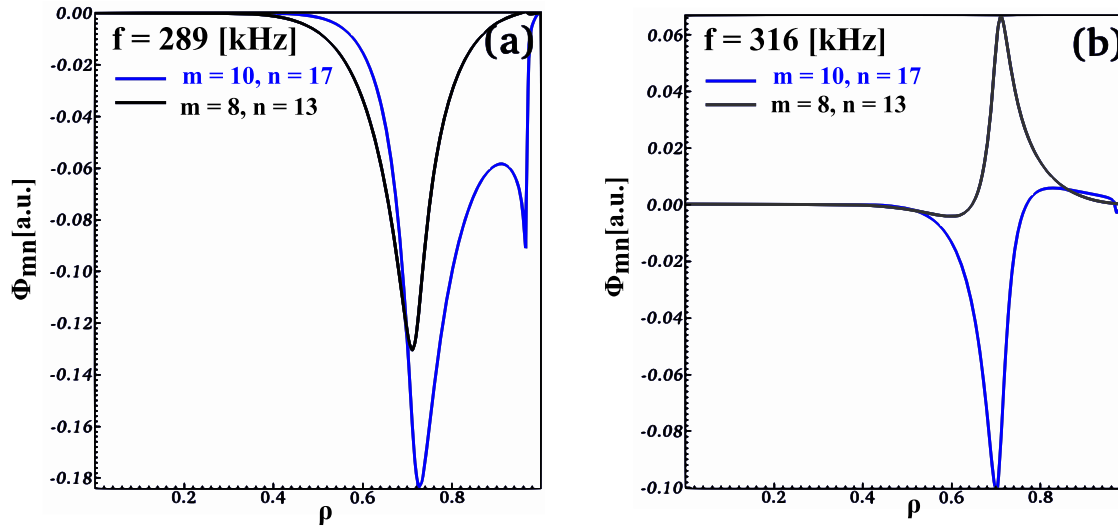


Figure 8. Alfvén eigenmodes for the chirping mode in discharge #29839. (a) An AE with two different sets of prominent mode numbers (m, n) having single dominant frequency 289 kHz and (b) AE with two different sets of prominent mode numbers (m, n) having single dominant frequency of 316 kHz.

different prominent modes. One of them having $m = 8$ and $n = 13$ is same and second one with dominant mode numbers $m = 12$ and $n = 21$ is unique as compared with the last two cases of discharge #29839. Both of these modes have same frequency of 334 kHz which is relatively higher than the prior cases at $t = 1150$ and 1160 ms. These modes are located radially further outwards at $\rho = 0.8$ than the modes at the previous time points.

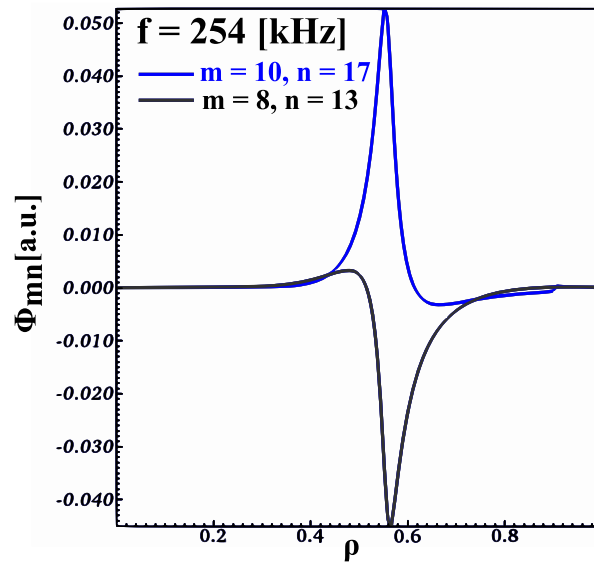


Figure 9. Alfvén eigenmodes for steady mode in discharge #29839. An AE with two different sets of prominent mode numbers (m, n) having single dominant frequency 254 kHz

We also have carried out simulations to check the Alfvénic character of the modes. For this purpose we have performed simulations at different electron densities. We find that the calculated mode frequency scales as $1/\sqrt{n_e}$ which confirms the Alfvénic character of the mode (c.f. Figure 10)

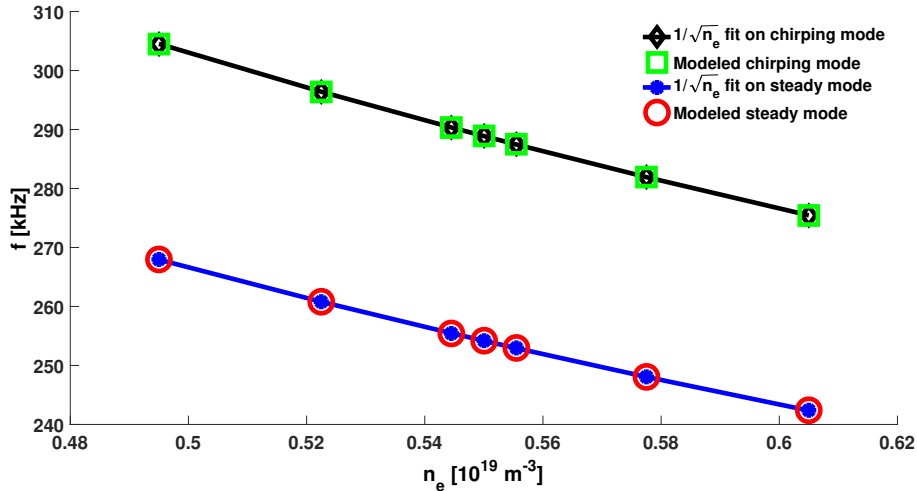


Figure 10. Frequency of the prominent modes as given by the AE3D code for discharge #29839 as a function of the electron density compared with the Alfvénic density scaling of the frequency as $1/\sqrt{n_e}$

6. Wave-particle resonances in TJ-II

To assess the phase space region of the neutral beam injected fast ions which provides the main contribution to the wave-particle interaction, a resonance map of contours of,

$$\Omega \equiv \omega - n\omega_\phi - p\omega_\theta = 0 \quad (4)$$

was computed with the particle-following code DELTA5D [21,22] for the beam injection geometry and magnetic equilibrium specific for the chosen time slices of interest. Here, ω_ϕ and ω_θ are the toroidal orbit frequency and the poloidal precession frequencies of the beam ions, respectively, n and ω are toroidal mode number and frequency of the AE, respectively, and integer p is the bounce harmonic. For assessing the resonances for the AEs found at different radii, beam particles were launched from the positions of $\rho = 0.25, 0.55$ and 0.75 .

For each value of ρ , fast hydrogen ions were launched in the range of energies $5 \text{ keV} < E < 20 \text{ KeV}$ and pitch-angles $1 \text{ T} < E/\mu < 9 \text{ T}$. For every fast ion launched, the corresponding drift orbit were computed assuming unperturbed particle motion, and the characteristic frequencies ω_ϕ and ω_θ were found as 2D functions of fast-ion energy and pitch-angle. The obtained 2D matrices for poloidal and toroidal frequencies of the drift orbits are shown in figures 11- 13. As ρ increases from 0.25 (Figure 11) to

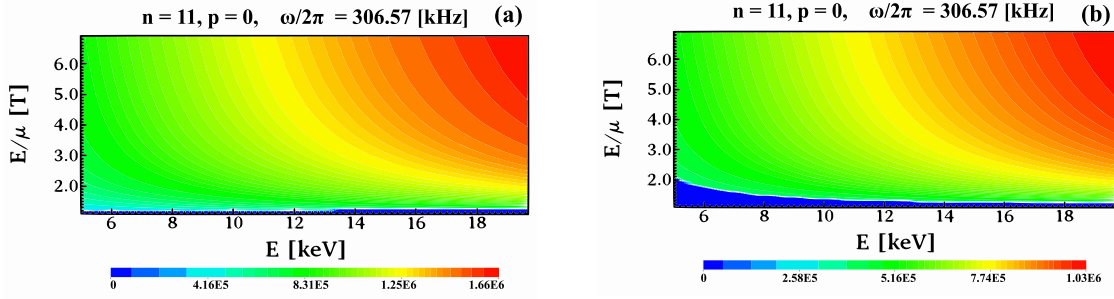


Figure 11. Contour plots of fast-ions energy and pitch angle for the the beam ions launched at $\rho = 0.25$. Contour plots of (a) poloidal orbit frequency ω_θ and (b) the toroidal precession frequency ω_ϕ

0.55 (Figure 12), and then to 0.75 (Figure 13), the area of unconfined beam ions as indicated by the blue area expands, effectively pushing the phase space area of confined beam ions down to lower energies. Using the calculated poloidal orbit frequency and the toroidal precession frequency, one can now combine their 2D functions in the form (4) for various integer values of p and for the frequency and toroidal mode number of the AE of interest. The resulting 2D function is then the resonance map, showing the phase space regions involved in the wave-particle resonance as a function of energy and pitch-angle. Figure 14 shows one of the resonance maps relevant to the core-localised AE with a frequency of 306.57 kHz, for $p = 0$ and $n = 11$ for beam ions launched at $\rho = 0.25$.

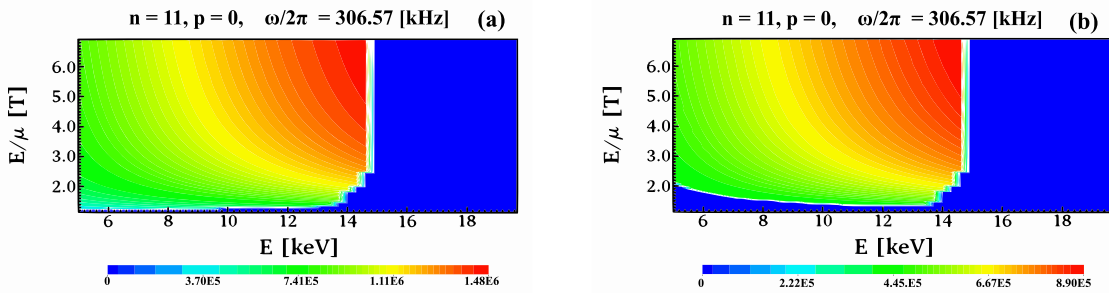


Figure 12. Contour plots of fast-ions energy and pitch angle for the the beam ions launched at $\rho = 0.55$. Contour plots of (a) poloidal orbit frequency ω_θ and (b) the toroidal precession frequency ω_ϕ

The special shape of the resonance map in figure 14 suggests a natural division of the resonant ions in two phase space regions. Region 1 (orange oval) is narrow in energy ($3 \text{ keV} < E < 4 \text{ keV}$), but insensitive to pitch angle, while region 2 (black oval) covers only a narrow range of pitch angles and extends in energy ($5 \text{ keV} < E < 12 \text{ keV}$). In region 1 the beam ions are affected by the electric field of the AEs, and are replenished due to the beam energy scattering and electron drag. In contrast to this, the region 2 replenishes by pitch-angle scattering (with a diffusive collisional operator). Therefore, in the case of the TJ-II resonance map, one arrives at the possibility of describing the

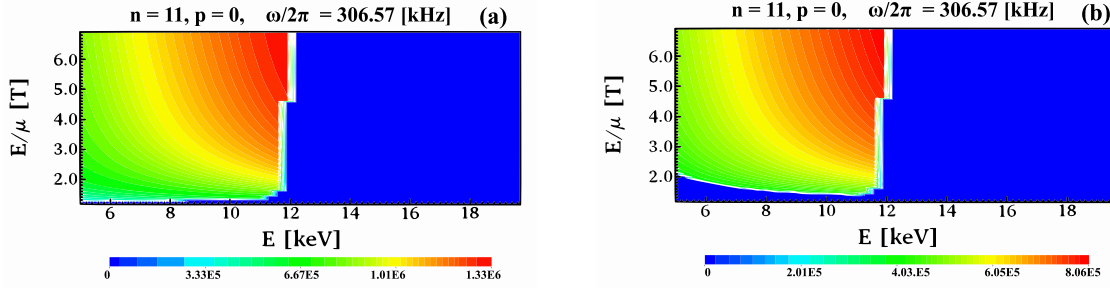


Figure 13. Contour plots of fast-ions energy and pitch angle for the the beam ions launched at $\rho = 0.75$. Contour plots of (a) poloidal orbit frequency ω_θ and (b) the toroidal precession frequency ω_ϕ

nonlinear evolution of the AEs by a sum of two ion populations with different weighting factors, one of which is dominated by drag and the other by diffusion.

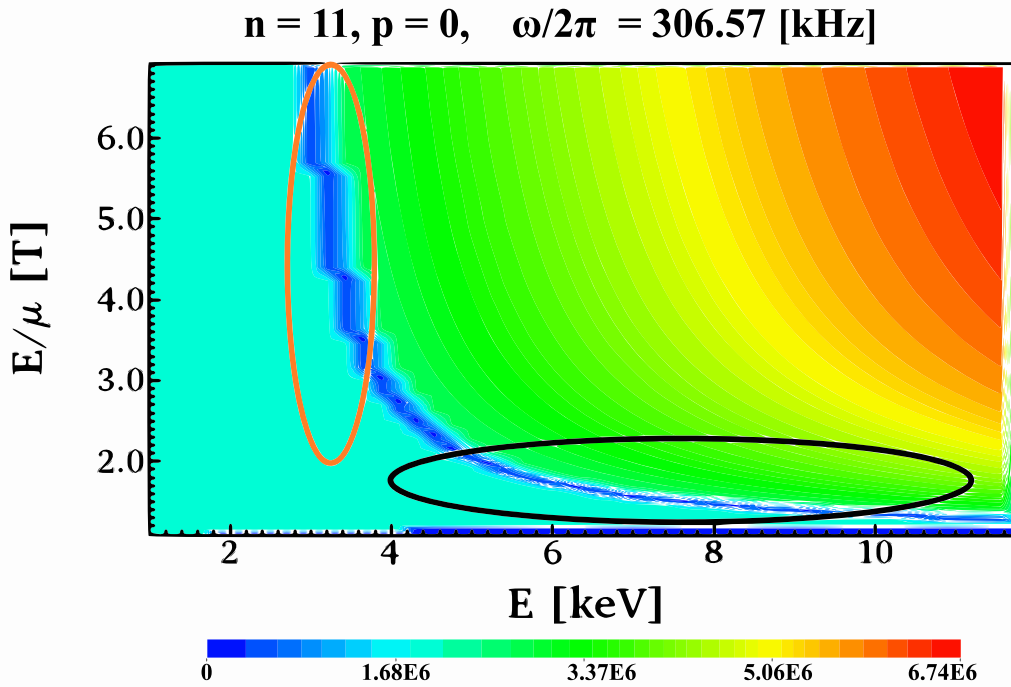


Figure 14. Resonance map $\Omega \equiv \omega - n\omega_\phi - p\omega_\theta = 0$ for the core-localised AE with a frequency of 306.57 kHz and $p = 0$ and $n = 11$ for beam ions launched at $\rho = 0.25$. The orange oval marks Region 1 which is narrow in energy, but insensitive to pitch angle. The black oval marks Region 2 which covers a narrow range of pitch angles and extends in energy

Figure 15 shows the orbits for two selected resonant fast ions as given by DELTA5D code in the drag and diffusion dominated regions of figure 14. Similar fast ion orbits were previously obtained with the ISDEP code for TJ-II [23, 24]. The modelled orbits are broadly similar in both regions and exhibit full sampling in both the poloidal and toroidal directions.

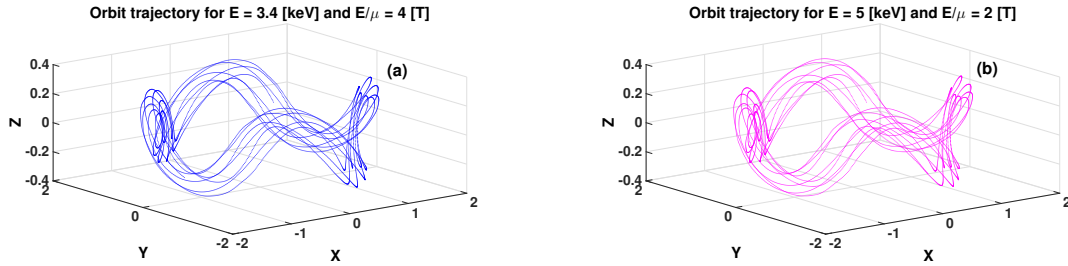


Figure 15. Orbit trajectories of two fast ions launched at $\rho = 0.25$ in TJ-II that are resonant with the core-localised AE with a frequency of 306.57 kHz and $p = 0$ and $n = 11$. (a) The orbits with $E = 3.4$ keV and $E/\mu = 4$ T are those from Regions 1 and (b) the orbits with $E = 5$ keV and $E/\mu = 2$ T are those from Regions 2, of the resonance map shown in figure 14.

It was found earlier in [25, 26] that the type of the replenishment (by drag or by diffusion) of an unstable energetic particle distribution determines the nonlinear evolution of energetic particle-driven modes. In particular, it was shown that the drag-dominated distribution at the resonance could not give a steady-state evolution of the mode. Further development of this theory was performed recently by [27] to include two species of the beam ions, one of which is reconstituted in the resonance area by drag only, and the other by diffusion only. New nonlinear scenarios of the mode evolution were found and, in particular, a transition from the steady-state nonlinear AE evolution to the sweeping frequency (chirping) AEs as the proportion between the two types of the resonating ions was varied slightly. It could be of particular interest for future studies to investigate whether the iota variation in TJ-II experiments could affect the proportion between the resonant beam particles in area I (drag-dominated region) and area II (diffusion-dominated region) so the scenario observed in [27] is reproduced.

7. Summary and conclusions

Our 3D modelling results for dominant modes are summarized in table 7. We find that the reduced MHD simulations agree with the mode characteristics as measured by the heavy ion beam probe (HIBP) diagnostic in discharges #29834 and #29839 at the specified times. The HIBP data show that modes are located around $\rho = 0.55$ and the frequencies of modes are around 295 kHz. Good agreement between simulations and experiments is found in the frequency and radial location of the modes.

Simulations show that the case with iota ramping down in time moves the modes towards the outboard side while a ramp-up in iota pushes them to the inboard side. The inward movement of the modes suggests that EP confinement is improving. Moreover, the AE frequencies show a ramp-up and ramp-down trend for iota ramp-down and ramp-up, respectively. The combination of the toroidal (n) and poloidal (m) mode numbers at different iota windows or, equivalently, at different time slices of discharge enhances the confidence of appearance of same mode, in agreement with the experimentally observed co-existence of the mode. The corresponding wave-particle resonance maps suggest the

Table 1. Summary of simulation results for the AE mode localizations and frequencies. Here, *s* and *c* correspond to the steady and chirping types of modes, respectively.

| Discharges | Modes (m, n) | Frequency(kHz) | Radial location(ρ) |
|------------|--------------------|---------------------------|---------------------------|
| #29834 | (11, 19) & (9, 15) | 276 (s), 256 (s) | 0.65 |
| | | 292 (c), 287 (c) | 0.75 |
| | (2, 3) | 272 (c), 275 (s) | 0.40 , 0.45 |
| #29839 | (10, 17) & (8, 13) | 316 (c), 289 (c), 254 (s) | 0.70 , 0.70 , 0.55 |
| | (8, 13) | 251 (s), 334 (c) | 0.55 , 0.80 |

possibility of describing the nonlinear evolution of the AEs in TJ-II by a sum of two ion populations with different weighting factors, one of which is dominated by drag and the other by diffusion.

Acknowledgments

This work has been carried out within the framework of the EUROfusion Consortium and has received funding from the Euratom research and training programme 2014-2018 under grant agreement No 633053. The views and opinions expressed herein do not necessarily reflect those of the European Commission. Allah Rakha is grateful to 'AGAUR FI predoctoral grant' for supporting his PhD studies. This work has received funding from the Spanish Ministry of Economy and Competitiveness (MINECO) under grant ENE2015-67371-R.

References

- [1] Kramer G.J. *et al* 2016 *Plasma Phys. Control. Fusion* **58** 085003
- [2] Jiménez-Gómez R. *et al* 2011 *Nucl. Fusion* **51** 033001
- [3] Kolesnichenko Ya. I. *et al* 2001 *Phys. Plasmas* **8** 491
- [4] Könies A. and Eremin D. 2010 *Phys. Plasmas* **17** 012107
- [5] Könies A. 2007 A code for the calculation of kinetic Alfvén waves in three-dimensional Geometry
10th IAEA TM on Energetic Particles in Magnetic Confinement Systems
- [6] Spong D. A., Sanchez R. and Weller A. 2003 *Phys. Plasmas* **10** 3217
- [7] Salat A. and Tataronis J. A. 2001 *Phys. Plasmas* **8** 1207
- [8] Spong D. A., D'Azevedo E. and Todo Y. 2010 *Phys. Plasmas* **17** 022106
- [9] Kruger S. E., Hegna C. C. and Callen J. D. 1998 *Phys. Plasmas* **5** 4169
- [10] Cook C. R. 2015 Shear Alfvén continua and discrete modes in the presence of a magnetic islands
PhD thesis, University of Wisconsin-Madison (2015)
- [11] Toi K. 2013 *Plasma and Fusion Research* **8** 1102002
- [12] Sun B. J., Ochando M.A. and López-Bruna D. 2015 *Nucl. Fusion* **55** 093023
- [13] Melnikov A.V. *et al* 2012 *Nucl. Fusion* **52** 123004
- [14] Castejón F. *et al* 2016 *Plasma Phys. Control. Fusion* **58** 094001
- [15] Melnikov A.V. *et al* 2016 *Nucl. Fusion* **56** 076001
- [16] Melnikov A.V. *et al* 2010 *Nucl. Fusion* **50** 084023
- [17] Melnikov A.V. *et al* 2014 *Nucl. Fusion* **54** 123002
- [18] Sleijpen G. L. G. and Van der Vorst H. A. 2000 *SIAM J. Matrix Anal. & Appl.* **17** 401-425

- [19] Hirshman S. P. and Whitson J. C. 1983 *Phys. Fluids* **26** 3553
- [20] Rakha A. *et al* 2018 Modelling of Alfvén cascades in NBI heated stellarator plasmas *45th EPS Conference on Plasma Physics, Prague, Czech Republic 2018*.
- [21] Fowler R. H., Rome J. A. and Lyon J. F. 1985 *Phys. Fluids* **28** 338
- [22] Spong D. A., Hirshman S. P. and Whitson J. C. 1997 *Plasma Phys. Rep.* **23** 483
- [23] Bustos A. *et al* 2011 *Nucl. Fusion* **51** 083040
- [24] Rodríguez-Pascual M. *et al* 2013 *Plasma Phys. Control. Fusion* **55** 085014
- [25] Lilley M.K., Breizman B.N. and Sharapov S.E. 2009 *Phys. Rev. Lett.* **102** 195003
- [26] Lilley M.K., Breizman B.N. and Sharapov S.E. 2010 *Phys. Plasmas* **17** 092305
- [27] Aslanyan V., Porkolab M., Sharapov S. E. and Spong D. A. 2017 *Phys. Plasmas* **24** 122511